Sodium and potassium vapor Faraday filters revisited: theory and applications

S. D. Harrell,[1,*] C.-Y. She,[1] Tao Yuan,[1] David A. Krueger,[1] H. Chen,[1,2] S. S. Chen,[1,3] and Z. L. Hu[1,4]

[1]*Department of Physics, Colorado State University, Fort Collins, Colorado 80523-1875, USA*
[2]*Present Address: NASA Goddard Space Flight Center, Code 613.1, Greenbelt, Maryland 20771, USA*
[3]*Present Address: Science Systems and Applications, Inc., Hampton, Virginia 23666, USA*
[4]*Present Address: Department of Biomedical Engineering, Case Western Reserve University, Cleveland, Ohio 44106, USA*
[*]*Corresponding Author: sharrell@lamar.colostate.edu*

Received September 8, 2008; revised January 15, 2009; accepted January 15, 2009; posted January 22, 2009 (Doc. ID 101306); published March 11, 2009

A complete theory describing the transmission of atomic vapor Faraday filters is developed. The dependence of the filter transmission on atomic density and external magnetic field strength, as well as the frequency dependence of transmission, are explained in physical terms. As examples, applications of the computed results to ongoing research to suppress sky background, thus allowing Na lidar operation under sunlit conditions, and to enable measurement of the density of mesospheric oxygen atoms are briefly discussed. © 2009 Optical Society of America

OCIS codes: 260.1440, 260.5430, 260.5740, 260.7490.

1. INTRODUCTION

Extremely narrowband optical filters are required in many situations for extracting useful signals in the presence of a broadband background. For signals at an atomic resonance, an advantage is attained by using the Faraday effect, which involves a circularly birefringent, dichroic medium between crossed polarizers, as shown in Fig. 1. This medium can be an atomic vapor in an axial magnetic field, causing a rotation of the polarization of light near an atomic resonance while the polarization of off-resonance light is unaffected. Advantages of the atomic vapor Faraday filter include its wide field of view, high background rejection, and high peak transmission [1]. These types of filters are particularly attractive, as the resulting bandwidth is only several gigahertz (1 GHz = 1.2 $\times 10^{-3}$ nm @ 600 nm) wide, about 400 times narrower than 1 nm bandwidth optical interference filters commercially available.

A Faraday filter of this type was first introduced by Ohman in 1956 [2]. Studies using a variety of atomic species have since been performed [1,3,4]. Specifically, filters for Na were developed by Agnelli *et al.* and Chen *et al.*, while studies of the relationship between vapor temperature and cell transmission were performed by Hu *et al.* and Zhang *et al.* for Na and K filters, respectively [5–8]. Our work has led to a Na vapor Faraday filter deployed in the Colorado State University Na lidar system [9], allowing the measurement of mesopause region (~90 km altitude) temperature and horizontal wind under sunlit conditions, thus permitting studies of the solar atmospheric tides and their variability [10].

Our current interest in the Faraday filter stems from ongoing development of a spectrometer to measure the Na nightglow D_2/D_1 intensity ratio in the mesopause region. Slanger *et al.* suggested that the varying D_2/D_1 results from variation in the ratio of the concentration of atomic oxygen to the concentration of molecular oxygen $[O]/[O_2]$ due to competing chemical processes [11]. Measuring the variation between the two chemical pathways requires an extremely high resolution spectrometer—on the order of the bandwidth of a Faraday filter. By using a pair of Faraday filters, with their transmission functions independently optimized as will be shown, we can determine valuable information on the important atomic oxygen concentration.

Designing the spectrometer requires theoretical calculations of filter transmissions. Analysis of available literature showed that most publications are either missing complete derivations or are not easily adaptable to different situations, thus limiting their usefulness. For example, Yeh and Van Baak provide only a limited treatment of the quantum mechanical description of atomic states, ignoring the hyperfine structure, while Dressler *et al.* give a detailed solution, but only for weak external magnetic fields, which is unsuitable for our high-field application [12–14]. Yin and Shay present a theory valid for arbitrary magnetic field for a cesium Faraday filter operating at the Cs D_2 line, but their letter lacks detail to make it useful for others to replicate [15]. This paper not only details the complete calculation of Faraday filter transmission, which is applicable to all values of external magnetic field, but our results are also readily adaptable for other applications.

In Section 2, we detail the classical calculation of the filter transmission and then relate this to the quantum-mechanical derivation of the complex susceptibility in Section 3. Section 4 explains the theoretical results for both Na and K and contains tabulated current values for all relevant constants and coefficients. Appendix A contains the calculation of transition matrix elements.

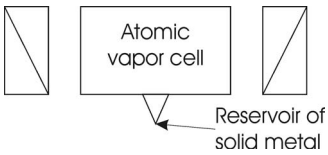

Fig. 1. Schematic of an atomic vapor Faraday filter, consisting of a vapor cell in an axial magnetic field between crossed polarizers.

2. CLASSICAL THEORY: FILTER TRANSMISSION

To calculate filter transmission, we express the optical response of the medium in terms of a complex susceptibility $\chi_\pm(\omega)=\chi'_\pm+i\chi''_\pm$, where the $\pm$ represents left- and right-handed circular polarizations of the incident light. The complex susceptibility relates the wavenumber k and angular frequency ω in the dispersion relation, since

$$k=\frac{\omega}{c}\sqrt{(1+\chi'_\pm+i\chi''_\pm)}\approx\frac{\omega}{c}\left(1+\frac{\chi'_\pm}{2}+i\frac{\chi''}{2}\right), \tag{1}$$

where c is the speed of light. This is valid for relatively low vapor density, a situation suitable for most applications. The quantum mechanical derivation of $\chi_\pm(\omega)$ is given in Section 3.

After the first polarizer of the Faraday filter, the randomly polarized input electric field, entering from the left of Fig. 1, is linearly polarized, which we denote as the $\hat{x}$ direction. The two linear polarizations ($\hat{x}$ and $\hat{y}$) can be expressed as a sum of circular polarizations written in terms of circular polarization $\hat{+}$ and $\hat{-}$ coordinates:

$$\hat{x}=-\frac{\hat{+}-\hat{-}}{\sqrt{2}},\quad\text{and}\ \hat{y}=i\frac{\hat{+}+\hat{-}}{\sqrt{2}}. \tag{2}$$

The input electric field, $\mathbf{E}(z,t)=\frac{1}{2}[\mathfrak{E}(z,\omega)e^{-i\omega t}+\mathfrak{E}^*(z,\omega)e^{i\omega t}]$, enters the vapor cell at $z=0$ and $t=0$. After a cell length $z=L$ and time t, the light will have passed through the vapor cell and the electric field will be

$$\mathfrak{E}(L,\omega)=-\frac{E_0}{\sqrt{2}}\left[\exp\left(i\left\{\frac{\omega}{c}(1+0.5\chi'_++0.5i\chi''_+)L\right\}\right)\hat{+}-\exp\left(i\left\{\frac{\omega}{c}(1+0.5\chi'_-+0.5i\chi''_-)L\right\}\right)\hat{-}\right], \tag{3}$$

which contains (for each circular polarization) an exponential decay or absorption term depending on χ'', and an oscillatory term depending on $1+0.5\chi'$—this is the index of refraction.

A second, crossed polarizer will select the light polarized in the $\hat{y}$ direction, so the transmission coefficient will be

$$\mathfrak{T}(\nu)=\frac{|\mathfrak{E}\cdot\hat{y}|^2}{E_0^2}=\frac{1}{4}\left[\exp\left(-\frac{\omega}{c}\chi''_+L\right)+\exp\left(-\frac{\omega}{c}\chi''_-L\right)-2\exp\left(-\frac{\omega}{c}\frac{\chi''_++\chi''_-}{2}L\right)\cos\left(\frac{\omega}{c}\frac{\chi'_+-\chi'_-}{2}L\right)\right]. \tag{4}$$

We can define the Faraday rotation θ_F as the angle of polarization rotation of the output light relative to the initial linear polarization:

$$\theta_F=\frac{\omega}{c}\frac{\chi'_+-\chi'_-}{4}L=\frac{\pi}{2\lambda}(\chi'_+-\chi'_-)L=\frac{\pi}{\lambda}(\Delta n)L, \tag{5}$$

where Δn is the difference in the index of refraction of the two circular polarizations (i.e., circular birefringence).

3. QUANTUM-MECHANICAL THEORY

A. Derivation of Susceptibility

Since an atomic vapor is an ensemble of many atoms, its state may be represented by a density matrix: $\rho=\Sigma_n|\psi_n\rangle p_n\langle\psi_n|$ [16]. To model the interaction of the atom in an external magnetic field, perturbation theory is used. The Schrödinger equation for the evolution of the density matrix of a system with Hamiltonian $H_0+\gamma H^I$, including a damping term to model interactions such as collisions, is

$$\frac{d\rho_{\alpha\beta}(t)}{dt}=\frac{1}{i\hbar}\{[H_0,\rho(t)]_{\alpha\beta}+[\gamma H^I(t),\rho(t)]_{\alpha\beta}\}+\left.\frac{\partial\rho_{\alpha\beta}}{\partial t}\right|_{\text{random}}=\frac{1}{i\hbar}\{\hbar\omega_{\alpha\beta}\rho_{\alpha\beta}+[\gamma H^I(t),\rho(t)]_{\alpha\beta}\}-\Gamma_{\alpha\beta}\rho_{\alpha\beta}(t), \tag{6}$$

where $\rho_{\alpha\beta}(t)$ represents an element of the density matrix between energy eigenstates of H_0, α, and β, where $\omega_{\alpha\beta}$ is the associated transition frequency. The damping constant $\Gamma_{\alpha\beta}$ is the natural linewidth of the transition. This means that $\Gamma_{\alpha\beta}/\pi=A_{\alpha\beta}/(2\pi)$, where $A_{\alpha\beta}$ is the Einstein coefficient for the transition rate between the two states. H_0 is the base Hamiltonian, and $H^I(t)$ is the interaction Hamiltonian, with γ being the strength of the perturbation.

In perturbation theory, $\rho_{\alpha\beta}$ can be expressed in the form of a power series, $\rho_{\alpha\beta}(t)=\Sigma_{i=0}^{\infty}\gamma^i\rho_{\alpha\beta}^{(i)}$, with each term obtained from a hierarchy of equations; the first-order equation is

$$\frac{d\rho_{\alpha\beta}^{(1)}(t)}{dt}=\frac{1}{i\hbar}\{\hbar\omega_{\alpha\beta}\rho_{\alpha\beta}^{(1)}(t)+[H^I(t),\rho^{(0)}]_{\alpha\beta}\}-\Gamma_{\alpha\beta}\rho_{\alpha\beta}^{(1)}(t). \tag{7}$$

For the electric dipole approximation, $H^I(t)=-e\mathbf{r}\cdot\mathbf{E}(t)=-\frac{e}{2}\Sigma_k r^k[\mathfrak{E}^k(\omega)e^{-i\omega t}+\mathfrak{E}^{*k}(\omega)e^{i\omega t}]$, with $-er_{\alpha\beta}^k=-e\langle\alpha|r^k|\beta\rangle$ as the electric dipole moment of an atomic electron with charge e connecting the $|\alpha\rangle$ and $|\beta\rangle$ eigenstates, and $\mathbf{E}(t)$ being the electric field of light propagating along the axis of the Faraday filter. Defining

$$\rho_{\alpha\beta}^{(1)}(t)=\frac{1}{2}[\rho_{\alpha\beta}^{(1)}(\omega)e^{-i\omega t}+\rho_{\alpha\beta}^{(1)*}(\omega)e^{i\omega t}], \tag{8}$$

the solution to Eq. (7) is

$$\rho_{\alpha\beta}^{(1)}(\omega)=\frac{1}{\hbar}\sum_{k=x,y}\frac{e(r_{\alpha\beta}^k\rho_{\beta\beta}^{(0)}-\rho_{\alpha\alpha}^{(0)}r_{\alpha\beta}^k)\mathfrak{E}^k}{\omega-\omega_{\alpha\beta}+i\Gamma_{\alpha\beta}}. \tag{9}$$

The expectation value of the polarization is

$$\mathbf{P}(t) = \langle -Ne\mathbf{r}\rangle = -Ne\mathrm{Tr}[\rho^{(1)}(t)\mathbf{r}] = \frac{1}{2}[\mathcal{P}(\omega)e^{-i\omega t} + \mathcal{P}^*(\omega)e^{+i\omega t}]. \tag{10}$$

To avoid confusion in notation, we decompose the vectors, $\mathbf{P}(\omega)$, $\mathbf{E}(\omega)$, and $\mathbf{r}$ into Cartesian coordinates. For an isotropic medium, both the polarization and electric field are transverse to the propagation direction $\hat{z}$, so combining Eqs. (9) and (10) gives

$$\mathcal{P}_j(\omega) = -\frac{Ne^2}{\hbar}\sum_{\alpha,\beta,k}\frac{(\rho^{(0)}_{\beta\beta} - \rho^{(0)}_{\alpha\alpha})r^j_{\beta\alpha}r^k_{\alpha\beta}E^k(\omega)}{\omega - \omega_{\alpha\beta} + i\Gamma_{\alpha\beta}}. \tag{11}$$

where j and k represent the components $(\hat{x},\hat{y})$.

Due to the axial symmetry of the magnetic field, the circular polarizations are eigenmodes of the system. We can transform the Cartesian coordinates into circular polarizations using (2), and rewriting (11) in terms of the relevant dipole moment, $-er^{\pm}_{\alpha\beta} = -e\langle\alpha|r^{\pm}|\beta\rangle$, transition frequency, $\omega^{\pm}_{\alpha\beta}$, and damping constant, $\Gamma^{\pm}_{\alpha\beta}$. We then have:

$$\begin{aligned}\mathcal{P}_{\pm}(\omega) &\equiv \varepsilon_0\chi^{(1)}_{\pm}(\omega)\mathcal{E}_{\pm}(\omega) \rightarrow \chi^{(1)}_{\pm}(\omega)\\ &= -\frac{Ne^2}{\varepsilon_0\hbar}\sum_{\alpha\beta}\frac{(\rho^{(0)}_{\beta\beta}|(r^{\pm})_{\beta\alpha}|^2 - \rho^{(0)}_{\alpha\alpha}|(r^{\pm})_{\alpha\beta}|^2)}{\omega - \omega^{\pm}_{\alpha\beta} + i\Gamma^{\pm}_{\alpha\beta}}.\end{aligned} \tag{12}$$

By assuming that in the zero-order, only the ground state is populated, we can rewrite Eq. (12) (replacing β with g for "ground state"):

$$\chi^{(1)}_{\pm}(\omega) = -\frac{Ne^2}{\varepsilon_0\hbar}\sum_{\alpha g}\rho^{(0)}_g|r^{\pm}_{\alpha g}|^2\left(\frac{1}{\omega - \omega^{\pm}_{\alpha g} + i\Gamma^{\pm}_{\alpha g}} - \frac{1}{\omega + \omega^{\pm}_{\alpha g} + i\Gamma^{\pm}_{\alpha g}}\right), \tag{13}$$

where $\omega^{\pm}_{\alpha g} = -\omega^{\pm}_{g\alpha}$ and $\Gamma^{\pm}_{\alpha g} = \Gamma^{\pm}_{g\alpha}$ have been assumed.

Since the resonance line is narrow ($\Gamma^{\pm}_{\alpha g} \ll \omega$), and for the range of frequencies of interest, $\omega + \omega^{\pm}_{\alpha g} \approx 2\omega^{\pm}_{\alpha g} \gg \Gamma^{\pm}_{\alpha g}$, Eq. (13) reduces to

$$\chi^{(1)}_{\pm}(\omega) = \frac{Ne^2}{\varepsilon_0\hbar}\sum_{\alpha g}\rho^{(0)}_g|(r^{\pm})_{\alpha g}|^2\left(\frac{2\omega^{\pm}_{\alpha g}}{2\omega^{\pm}_{\alpha g}(\omega^{\pm}_{\alpha g} - \omega - i\Gamma^{\pm}_{\alpha g})}\right). \tag{14}$$

Including a Doppler broadening due to an atom's random motion with Gaussian distributed line of sight speed v, Eq. (14) becomes

$$\chi^{(1)}_{\pm}(\nu) = \frac{N}{2\pi\varepsilon_0\hbar}\frac{1}{\sqrt{\pi}u}\sum_{\alpha g}\rho^{(0)}_{\alpha g}\int_{-\infty}^{\infty}\frac{|(p_{\pm})_{\alpha g}|^2\exp(-\mathrm{v}^2/u^2)\mathrm{dv}}{[\nu^{\pm}_{\alpha g} - (\mathrm{v}/\lambda) - \nu - i(\Gamma^{\pm}_{\alpha g}/2\pi)]}, \tag{15}$$

where $u = \sqrt{2k_BT/m}$, and k_B, T, and m are respectively, the Boltzmann constant, temperature, and atomic mass. We have also replaced $e^2|r^{\pm}_{\alpha g}|^2$ with $|(p_{\pm})_{\alpha g}|^2$ for electric dipole moment. The integral in Eq. (15) is the complex Faddeeva function [17] and can be rewritten in real and imaginary components as

$$\chi'_{\pm}(\nu) = \frac{N}{2\pi\varepsilon_0\hbar}\frac{1}{\sqrt{\pi}u}\sum_{\alpha g}\rho^{(0)}_{\alpha g} \times \int_{-\infty}^{\infty}\frac{|(p_{\pm})_{\alpha g}|^2(\nu^{\pm}_{\alpha g} - (\mathrm{v}/\lambda) - \nu)\exp(-\mathrm{v}^2/u^2)\mathrm{dv}}{[(\nu^{\pm}_{\alpha g} - (\mathrm{v}/\lambda) - \nu)^2 + (\Gamma^{\pm}_{\alpha g}/2\pi)^2]}, \tag{16}$$

$$\chi''_{\pm}(\nu) = \frac{N}{2\pi\varepsilon_0\hbar}\frac{1}{\sqrt{\pi}u}\sum_{\alpha g}\rho^{(0)}_{\alpha g} \times \int_{-\infty}^{\infty}\frac{|(p_{\pm\alpha g})|^2(\Gamma^{\pm}_{\alpha g}/2\pi)\exp(-\mathrm{v}^2/u^2)\mathrm{dv}}{[(\nu^{\pm}_{\alpha g} - (\mathrm{v}/\lambda) - \nu)^2 + (\Gamma^{\pm}_{\alpha g}/2\pi)^2]}. \tag{17}$$

In practice, the ground state is a multiplet, and the factor $\rho^{(0)}_g$ takes into account any differences in fractional population in the various ground states. From Maxwell–Boltzmann statistics, $\rho^{(0)}_g$ is

$$Z = \sum_{i=1}^{N}\exp\left(-\frac{E_i}{k_BT}\right) \rightarrow \rho_g{}^{(0)} = \frac{N_i}{N_g} = \frac{\exp\left(-\frac{E_i}{k_BT}\right)}{Z}, \tag{18}$$

where E_i, not to be confused with the electric field, is the ground-state energy eigenvalue from Appendix A.

B. Derivation of Transmission Matrix Elements

The Hamiltonian governing the splitting of individual energy levels due to the hyperfine structure and Zeeman splitting is [18]

$$\begin{aligned}H &= H_0 + H^I\\ H^I &= H_{\mathrm{HFS}} + H_{\mathrm{Zeeman}}\\ &= A_J(\mathbf{I}\cdot\mathbf{J}) + \frac{B_J}{2I(2I-1)J(2J+1)}\\ &\quad\times\left[3(\mathbf{I}\cdot\mathbf{J})^2 + \frac{3}{2}(\mathbf{I}\cdot\mathbf{J}) - I(I+1)J(J+1)\right]\\ &\quad + g_J\mu_B\mathcal{B}_0\mathbf{J} - g_I\mu_N\mathcal{B}_0\mathbf{I},\end{aligned} \tag{19}$$

where H_0 and H^I are the base and interaction Hamiltonians, respectively. The parameters A_J and B_J represent the strength of the hyperfine magnetic dipole and electric quadrupole interactions; vectors $\mathbf{I}$ and $\mathbf{J}$ are the nucleus and electron total angular momentum operators with magnitudes I and J; μ_B and μ_N are the Bohr and nuclear magnetons; $\mathcal{B}_0$ is the external magnetic field strength; and g_J and g_I are the Lande-g factors of the atom and of the nucleus; g_J may be related to J, orbital angular momentum L, and electron spin S as [19]

$$g_J = \frac{3J(J+1) + S(S+1) - L(L+1)}{2J(J+1)}. \tag{20}$$

In order to evaluate the transition matrix element of the dipole moment in Eq. (15) and the energies of the eigenstates, we must first solve the eigenvalue problem of the individual atomic states. The first step is to choose a

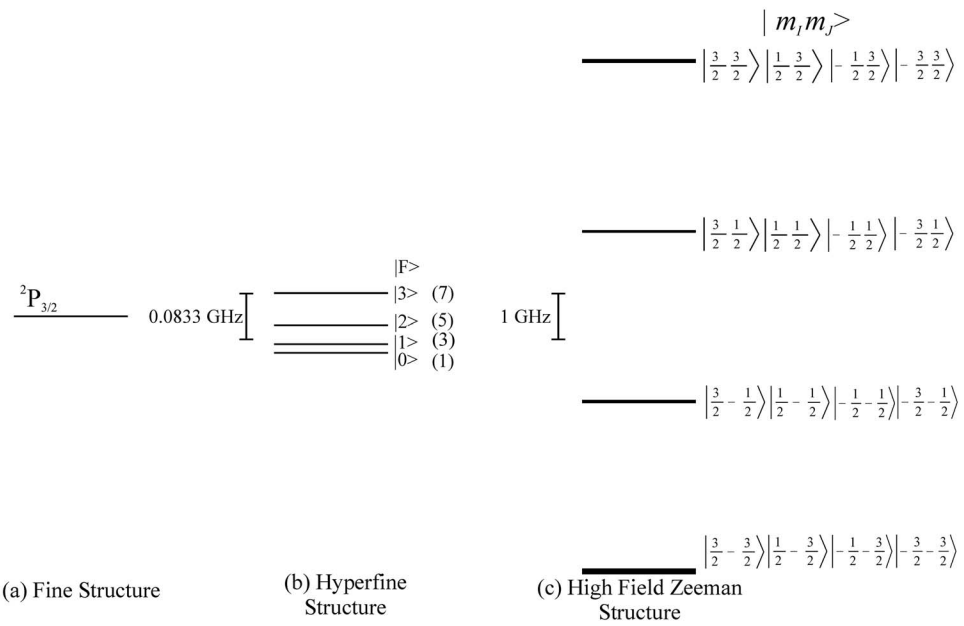

Fig. 2. Energy level diagram for Na showing the $3^2P_{3/2}$ excited states. (a) The single fine structure state, with a degeneracy of 16. (b) The hyperfine splitting case with no external magnetic field. The $|F\rangle$ eigenstate notation and degeneracies (in parentheses) are indicated to the right, and the scale in GHz is to the left. (c) The exact solution for the Zeeman structure for an external magnetic field of 2000G. The states are broken up into four closely spaced groups due to the different values for μ_I and μ_B. Each Zeeman state has a degeneracy of 1. The $|m_I\ m_J\rangle$ eigenstate notations are listed to the right, and the scale in GHz is to the left.

set of basis states; here the unperturbed Hamiltonian includes the Coulomb attraction of the nucleus and the interactions between atomic electrons. Thus the eigenstates of H_0 are $|I\ J\ m_I\ m_J\rangle$ with total electronic angular momentum and nuclear spin as good quantum numbers, and they have a degeneracy of $(2J+1)(2I+1)$. Under the influence of H^I, some of the degeneracy will be lifted. In the limit of zero (or low) magnetic field, the coupling between the atomic electrons and the nucleus will be dominant, and the eigenstates of H_0+H_{HFS} are $|I\ J\ F\ m_F\rangle$, with the total angular momentum of the atom (including the nucleus) $\mathbf{F}=\mathbf{I}+\mathbf{J}$; the energy eigenvalues will then depend on the strengths of hyperfine interactions, A_J and B_J. In the limit of high magnetic field, its interaction with the atom will cause $\mathbf{I}$ and $\mathbf{J}$ to align to the external field separately. This would allow the use of $|I\ J\ m_I\ m_J\rangle$ as the eigenstates of H_0+H_{Zeeman}; however, to account for hyperfine interactions, the eigenvalues should include the diagonal contribution from H_{HFS} as an approximation. For a solution valid at all values of magnetic field strength, an appropriate choice would be $|I\ J\ Q\ m_Q\rangle$, which reduces to $|I\ J\ Fm_F\rangle$ in the low or zero field limit, and to $|I\ J\ m_I\ m_J\rangle$ in the high field limit. For simplicity we choose to write the $|J\ I\ Q\ m_Q\rangle$ states as a linear superposition of $|I\ J\ m_I\ m_J\rangle$ states [18]. The total Hamiltonian in this representation is not diagonal; it must then be diagonalized to obtain the eigenstates and eigenvalues of the system. Figure 2 shows an example of splitting in the zero field limit (middle column) and the high field limit (right column) for the sodium $^2P_{3/2}$ excited state.

The solution for energy eigenvalues and eigenvectors and for transition matrix elements is in Appendix A. With the electric dipole matrix transition elements, $|(p_\pm)_{\alpha g}|$, evaluated, Eqs. (16) and (17) may be used to calculate χ' and χ'', from which θ_F and $\mathfrak{F}(\nu)$ may be calculated via Eqs. (4) and (5).

4. SAMPLE RESULTS AND DISCUSSION

A computer program was written in the Interactive Data Language (IDL) [20], using built-in functions to calculate

Table 1. Atomic Properties[a]

	Na	K					K		
A	23			39			41		
Mass (u)	22.989768			38.963707			40.961825		
g_I	1.478392			0.26099			0.1432543		
Abundance	100%			93.26%			6.73%		
	A_J (GHz)	B_J (GHz)	g_J	A_J (GHz)	B_J (GHz)	g_J	A_J (MHz)	B_J (MHz)	g_J
$^2S_{1/2}$	0.8858130644	0	2	0.2308598601	0	2	0.1270069352	0	2
$^2P_{1/2}$	0.0944	0	2/3	0.027775	0	2/3	0.015245	0	2/3
$^2P_{3/2}$	0.018572	0.002723	4/3	0.006093	0.002786	4/3	0.003363	0.003351	4/3

[a]Values for mass are from [22], g_I are from [23], abundance are from [22], and A_J and B_J are from [24–27].

Table 2. Linestrength[a], Transition Vacuum Wavelength, and Linewidth

	Ref.	Na		K	
		D_1	D_2	D_1	D_2
λ (nm)	[28]	589.7558	589.1582	770.108	766.701
$S=2S_0$ ($e^2a_0^2$)	[29]	37.3	37.3	51.6	51.6
$\Delta\nu$ (GHz)	[28]	0.00977	0.00980	0.00608	0.00616

[a]Linestrength S_0 is defined in Appendix A.

eigenvalues and eigenstates, which agreed exactly with longhand calculations. The complex Faddeeva function was calculated using an algorithm reported by Schreier [17].

Filter transmissions and associated θ_F were calculated for both D_2 and D_1 transitions of Na and K. Tables 1 and 2 give the necessary constants and coefficients. Values of g_I were calculated using the method detailed in [21].

The presence of different isotopes will affect the values of the A_J and B_J constants and g_I values used in the calculation. Na has only one stable isotope with mass number $A=23$, so the calculation can be done exactly as described. K has two dominant stable isotopes, $A=39$ and $A=41$, and so χ for K becomes a sum over the two isotopes weighted by their abundances, 93.26% and 6.73%, respectively.

One parameter is yet to be defined: vapor density. The density of the atomic vapor is a function of its temperature and pressure. In our particular vapor cell, we control the temperature of the reservoir (see Fig. 1) containing

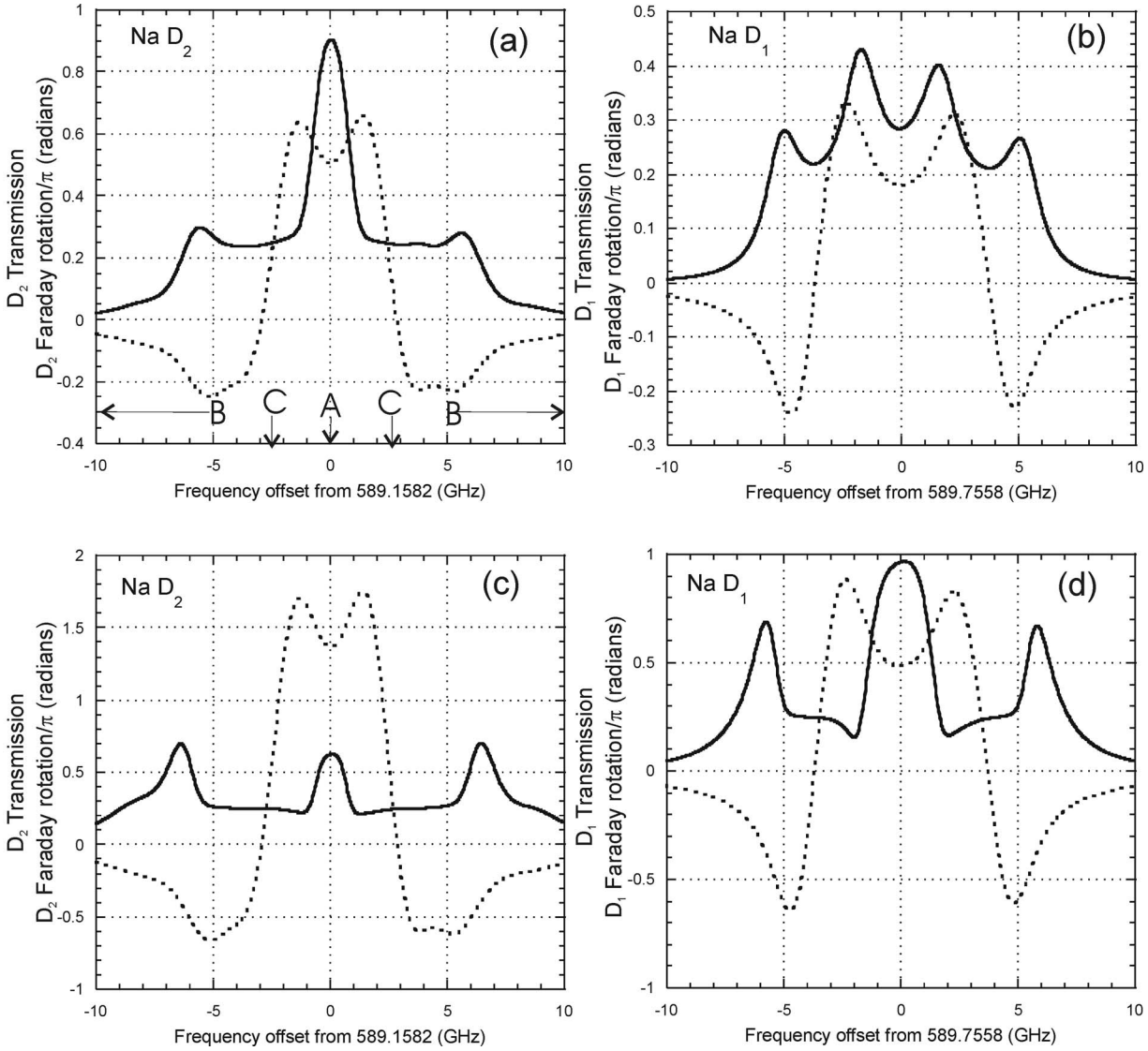

Fig. 3. (a) D_2 and (b) D_1 transmission as a fraction of input linear polarization (solid) and Faraday rotation in units of π (dashed) vs. frequency (GHz) for a Na vapor Faraday filter optimized for D_2. (c) and (d) are the same for a D_1 optimized filter. Filter parameters are listed in Table 3. The letters in (a) refer to the three cases described in the text.

solid and liquid Na (or K) to set the vapor pressure on the coexistence curve. Another controller fixes the temperature of the main body of the cell, which is the vapor temperature. From the ideal gas law the vapor density is proportional to this vapor pressure and inversely proportional to the temperature of the vapor. Data for vapor pressure as a function of saturated vapor temperature is given for both solid or liquid Na and K by Honig and Kramer [30], and we derived an equation using a curve-fit method similar to that described in [30]. For Na, the vapor pressure equation is

$$\log_{10}(P_{\mathrm{Na}}) = 71.899 - 9217.2(T_{\mathrm{res}})^{-1} + 40693000(T_{\mathrm{res}})^{-3} + 0.0061264(T_{\mathrm{res}}) - 9.6625\ln(T_{\mathrm{res}}), \quad (21)$$

and for K

$$\log_{10}(P_{\mathrm{K}}) = 69.53 - 10486(T_{\mathrm{res}})^{-1} + 1.8658 \times 10^{8}(T_{\mathrm{res}})^{-3} + 0.0027286(T_{\mathrm{res}}) - 8.5732\ln(T_{\mathrm{res}}), \quad (22)$$

where T_{res} is the temperature at the solid or liquid reservoir and P is the pressure in Torr.

Figures 3 through 6 show results calculated from the computer program, with the filter parameters listed in Table 3. Notice that the filter temperatures are chosen to respectively optimize the D_2 transition in parts (a) and (b) of Figs. 3 and 4 and to optimize the D_1 transition in parts (c) and (d) of Figs. 3 and 4. When mesospheric sodium nightglow is sent through the two Na Faraday filters with cell and reservoir temperature settings optimized to minimize error from photon noise, the detected signals may be processed to deduce Na D_2/D_1 ratio, thereby the ratio between the concentration of atomic oxygen to the concentration of molecular oxygen $[O]/[O_2]$.

In the curves for χ' and χ'', shown in Figs. 5 and 6, there are two groups of curves. Each set of curves is a summation of the curves for the various Zeeman split transitions with $\Delta m_J = \pm 1$, which is the selection rule for the circular $\hat{+}$ and $\hat{-}$ polarizations defined in Section 2. The central value of each group, indicated by the peak in the curve for χ'' or the zero crossing point of χ' is labeled as ν_0^- for the curves on the left and ν_0^+ for the curves on the right, and can be thought of as a resonance frequency for

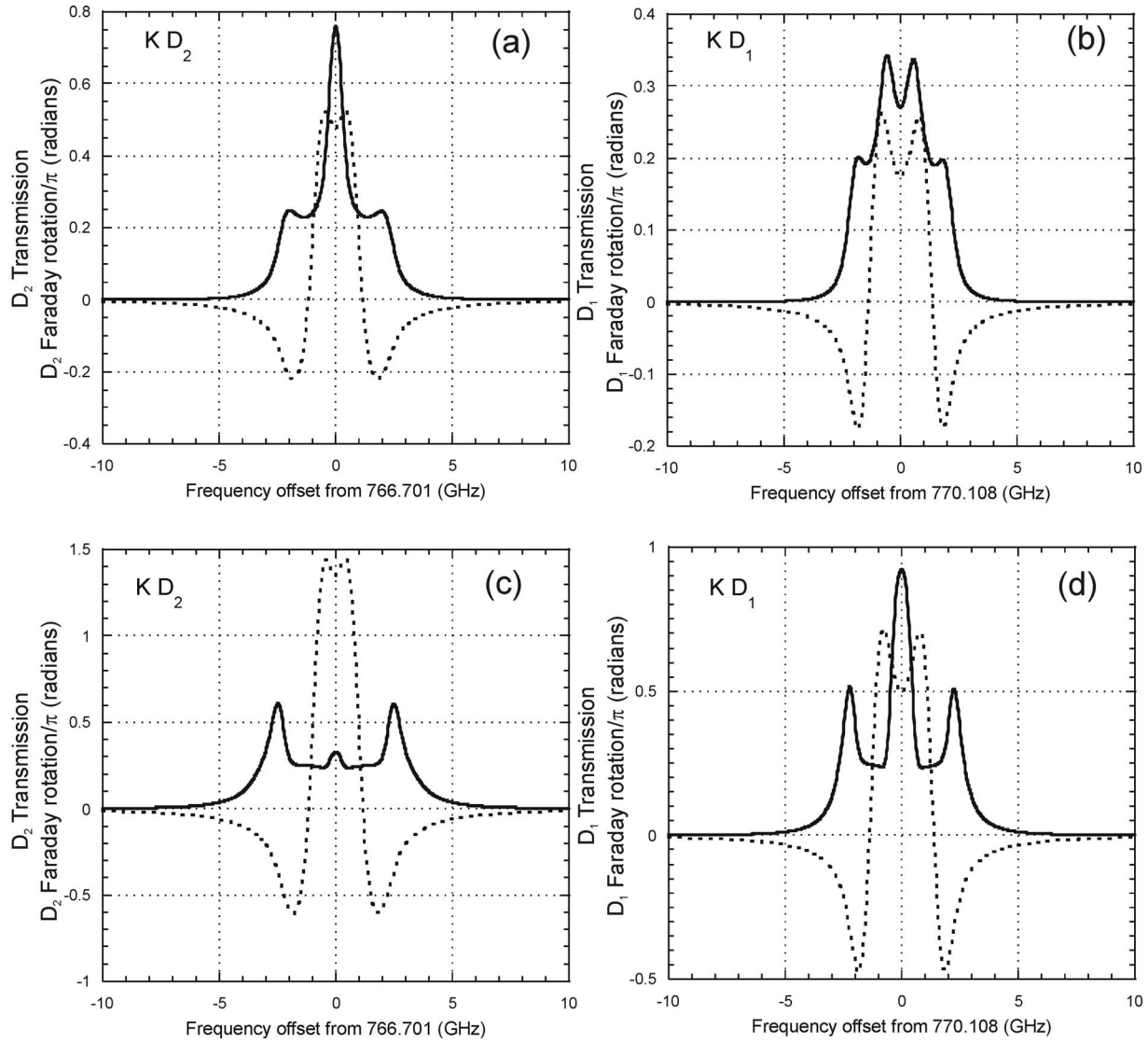

Fig. 4. Same as Fig. 3, except for K. Filter parameters are listed in Table 3.

Table 3. Filter Parameters used to Generate Figs. 2–5, and ν_0^+ and ν_0^- Transition Frequencies

	Na		K	
L (cm)	4			
$\mathcal{B}_0$ (G)	1850		700	
	D_1 optimized	D_2 optimized	D_1 optimized	D_2 optimized
T_{res} (°C)	180	164	94	76
T_{cell} (°C)	186	169	104	79
$D_1\nu_0^+$ (GHz)	3.6		1.3	
$D_1\nu_0^-$ (GHz)	−3.6		−1.3	
$D_2\nu_0^+$ (GHz)	2.5		1.0	
$D_2\nu_0^-$ (GHz)	−2.5		−1.0	

the circular polarization. This allows χ to be written as $\chi_\pm$ as was done in Eqs. (16) and (17) of Section 2.

By comparing the figures with the relevant equations, we can gain physical insight to what occurs in a Faraday filter. To facilitate this appreciation, we further consider the transmission function near three specific frequencies: A, at line center; B, off resonance; and C, at the resonance at either ν_0^+ or ν_0^- [see Fig. 3(a)]. For cases A and B, there is no absorption and the exponential factors in Eq. (4) are all unity, and the transmission reduces to $\mathfrak{F}(\nu)=\frac{1}{2}[1-\cos(2\theta_F)]=\sin^2\theta_F$. For case A the θ_F should be nonzero, since χ_+' and χ_-' are of opposite sign, and $\mathfrak{F}(\nu)$ varies periodically between 0 and near 1 as vapor density varies, so for fixed B_0 and cell length, we can easily adjust the vapor density to vary transmission at the line center. For case B, $\theta_F=0$, since far from resonance both χ_+' and χ_-' have the same value and $\mathfrak{F}(\nu)=0$. For case C, at ν_0^+ for example, χ_+' is zero. While χ_-'' is nonzero, χ_+'' is large enough to render

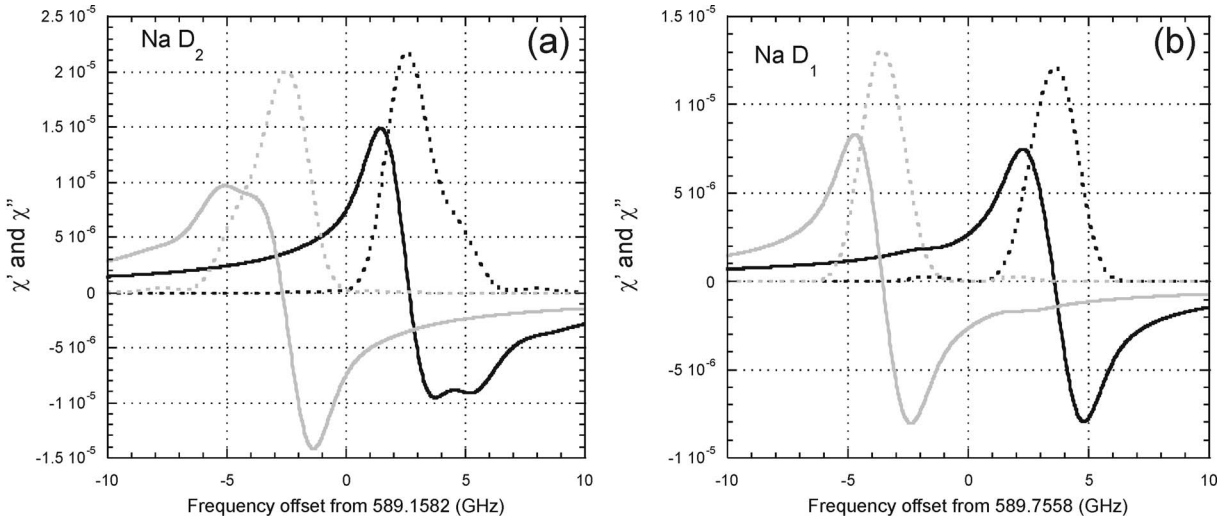

Fig. 5. χ' and χ'' curves for (a) Na D_2 and (b) D_1 lines split by the Zeeman effect due to the 1850 Gauss external magnetic field. Solid gray curve is χ' for σ_-, gray dashed curve is χ'' for σ_-, black solid curve is χ' for σ_+, and black dashed curve is χ'' for σ_+.

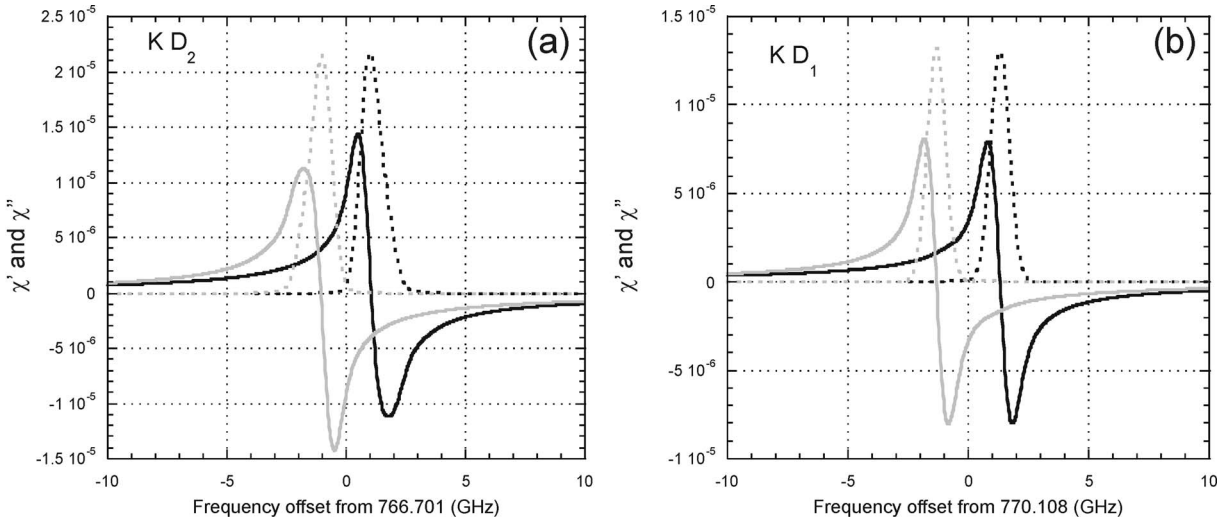

Fig. 6. Same as Fig. 5, only for K.

the associated exponential factors zero. In this case, one circular polarization is totally absorbed, and the electric field of the other polarization is reduced by the second polarizer by a factor of $\frac{1}{\sqrt{2}}$. Therefore, $\mathfrak{F}(\nu)\cong 0.25$ at either ν_0^+ or ν_0^-. In practice, the measured transmission can be scaled to $\frac{1}{4}$ at those frequencies to avoid the more involved normalization measurement described in [6].

5. CONCLUSIONS

We have presented a complete theory of the atomic vapor Faraday filter. In addition to upper atmospheric lidar, the results and associated computer program can now be used for various applications, including our studies of the physics and chemistry of the mesospause region. Other uses abound; Faraday filters can also be used to investigate Na and K atoms in the photosphere of the sun [5] and to investigate lower atmosphere winds with a sodium lidar [31], among other applications. The sample results presented help to further illustrate nuances in the theory. Our computer program can be made available on request. The approach in this paper is readily adaptable to other alkali atoms, which have the same electronic structure but different nuclear spin. For example, cesium has $I=7/2$ and, therefore, the degeneracy is doubled, but the electronic dipole transition probabilities, Eqs. (A5) and (A6) in Appendix A, are the same as Na and K.

APPENDIX A: TRANSMISSION MATRIX ELEMENT CALCULATIONS

1. Details of the Derivation of Transition Matrix Elements

The $|I\ J\ m_I\ m_J\rangle$ base states are now abbreviated $|m_J\ m_I\rangle$. As an example, the states $^2S_{1/2}$ and $^2P_{1/2}$ have $J=1/2$ ($I=3/2$ for Na and K). The set of 8 $|m_I\ m_J\rangle$ eigenstates is

$$\left[\left|\overset{1}{\tfrac{3}{2}}\overset{}{\tfrac{1}{2}}\right\rangle\left|\overset{2}{\tfrac{3}{2}}\overset{}{-\tfrac{1}{2}}\right\rangle\left|\overset{3}{\tfrac{1}{2}}\overset{}{\tfrac{1}{2}}\right\rangle\left|\overset{4}{\tfrac{1}{2}}\overset{}{-\tfrac{1}{2}}\right\rangle\left|\overset{5}{-\tfrac{1}{2}}\overset{}{\tfrac{1}{2}}\right\rangle\left|\overset{6}{-\tfrac{1}{2}}\overset{}{-\tfrac{1}{2}}\right\rangle\left|\overset{7}{-\tfrac{3}{2}}\overset{}{\tfrac{1}{2}}\right\rangle\left|\overset{8}{-\tfrac{3}{2}}\overset{}{-\tfrac{1}{2}}\right\rangle\right], \tag{A1}$$

and the numbers above the kets will be used as a simpler notation. We now proceed to solve the eigenvalue problem for the total Hamiltonian.

Raising and lowering operators $I_\pm$ and $J_\pm$ allows H^I to be written as a sum of three terms, according to the power of raising or lowering operators:

$$H_{\pm 0}=g_J\mu_B\mathcal{B}_0J_z-g_I\mu_I\mathcal{B}_0I_z+A_JI_zJ_z+\frac{B_J}{2I(I-1)J(2J-1)}\times\left[3\left(I_zJ_zI_zJ_z+\frac{1}{4}(I_+J_-I_-J_++I_-J_+I_+J_-)\right)+\frac{3}{2}I_zJ_z-I(I+1)J(J+1)\right],$$

$$H_{\pm 1}=\frac{A_J}{2}(I_+J_-+I_-J_+)+\frac{B_J}{2I(I-1)J(2J-1)}\frac{3}{2}\times\left[I_zJ_z(I_+J_-+I_-J_+)+(I_+J_-+I_-J_+)I_zJ_z+\frac{1}{2}(I_+J_-+I_-J_+)\right],$$

$$H_{\pm 2}=\frac{B_J}{2I(I-1)J(2J-1)}\frac{3}{4}(I_+J_-I_+J_-+I_-J_+I_-J_+). \tag{A2}$$

Continuing with the $^2S_{1/2}$ (or $^2P_{1/2}$) example, since there are 8 states, the Hamiltonian will be an 8×8 matrix in block-diagonal form with the subscripts using the notation of Eq. (A1):

$$H_{\mathrm{HFS}}=\begin{pmatrix} H_{1,1} & & & & & & & 0\\ & H_{2,2} & H_{2,3} & & & & & \\ & H_{3,2} & H_{3,3} & & & & & \\ & & & H_{4,4} & H_{4,5} & & & \\ & & & H_{5,4} & H_{5,5} & & & \\ & & & & & H_{6,6} & H_{6,7} & \\ & & & & & H_{7,6} & H_{7,7} & \\ 0 & & & & & & & H_{8,8}\end{pmatrix}. \tag{A3}$$

The values for the Hamiltonian matrix elements for these states of Na/K are listed here:

$$H_{1,1}=\frac{3}{4}A_J+\frac{1}{2}g_J\mu_B\mathcal{B}_0-\frac{3}{2}g_I\mu_n\mathcal{B}_0,$$

$$H_{6,6}=\frac{1}{4}A_J-\frac{1}{2}g_J\mu_B\mathcal{B}_0+\frac{1}{2}g_I\mu_n\mathcal{B}_0,$$

$$H_{2,2}=-\frac{3}{4}A_J-\frac{1}{2}g_J\mu_B\mathcal{B}_0-\frac{3}{2}g_I\mu_n\mathcal{B}_0,$$

$$H_{7,7}=-\frac{3}{4}A_J+\frac{1}{2}g_J\mu_B\mathcal{B}_0+\frac{3}{2}g_I\mu_n\mathcal{B}_0,$$

$$H_{3,3}=\frac{1}{4}A_J+\frac{1}{2}g_J\mu_B\mathcal{B}_0-\frac{1}{2}g_I\mu_n\mathcal{B}_0,$$

$$H_{8,8} = \frac{3}{4}A_J - \frac{1}{2}g_J\mu_B\mathcal{B}_0 + \frac{3}{2}g_I\mu_n\mathcal{B}_0,$$

$$H_{4,4} = -\frac{1}{4}A_J - \frac{1}{2}g_J\mu_B\mathcal{B}_0 - \frac{1}{2}g_I\mu_n\mathcal{B}_0,$$

$$H_{2,3} = H_{3,2} = H_{6,7} = H_{7,6} = \frac{\sqrt{3}}{2}A_J,$$

$$H_{5,5} = -\frac{1}{4}A_J + \frac{1}{2}g_J\mu_B\mathcal{B}_0 + \frac{1}{2}g_I\mu_n\mathcal{B}_0,$$

$$H_{4,5} = H_{5,4} = A_J. \tag{A4}$$

The blocks in the Hamiltonian matrices, at most 2×2, can be solved independently and easily, yielding energy eigenvalues E and eigenstates with their associated coefficients. The $^2P_{3/2}$ state can be solved similarly; however, it is a 16×16 block-diagonal matrix with a maximum block size of 4×4.

With the energy levels and eigenstate coefficients determined, we can calculate the transition frequencies and probabilities of the allowed transitions. The transitions of interest are electric dipole with selection rules $\Delta m_I = 0$ and $\Delta m_J = \pm1$ for absorption or emission of a circularly polarized photon in the filter. The transition probability is given by the square of the transition matrix element $|\langle m_I' m_J' | p_\pm | m_I m_J\rangle|^2$ where primed and unprimed represent excited and ground states. This may be written as product of 3-j symbols and the reduced matrix element $\langle I'J'\|p\|IJ\rangle$ [32]. This can be further reduced to the reduced matrix element between states in the "basic" model of the atom using 6-j symbols [33]. This basic-model reduced matrix element, $|\langle l'\|p\|l\rangle|^2$, is known as the line strength, S_0, of the transition; it is the total intensity of the line and is experimentally determined and tabulated in a National Bureau of Standards (NBS) publication [29] and reproduced in Table 2. The total transition probability of each Zeeman transition is given by

$$\begin{aligned}|\langle m_I' m_J' | p_\pm | m_I m_J\rangle|^2 &= |a|^2|b|^2(2J'+1)(2J+1)\\ &\times \begin{pmatrix} J' & 1 & J \\ -m_J' & \pm1 & m_J \end{pmatrix}^2 \begin{bmatrix} l' & J' & S \\ J & l & 1 \end{bmatrix}^2 S_0\\ &= F_1F_2(2J'+1)(2J+1)\begin{bmatrix} l' & J' & S \\ J & l & 1 \end{bmatrix}^2 S_0,\end{aligned} \tag{A5}$$

where a and b are the expansion coefficients of the appropriate eigenstate for the ground and excited states as defined above. The 3-j symbol is

$$\begin{pmatrix} J' & 1 & J \\ -m_J' & \pm1 & m_J \end{pmatrix}$$

and

Table 4. D_1 Allowed Transition F_1 Value and Polarization

$^2S_{1/2}$	$^2P_{1/2}$	F_1	Polarization
$\|3/2,1/2\rangle$	$b_{2-}\|3/2,-1/2\rangle + b_{2+}\|1/2,1/2\rangle$	$\|b_{2-}\|^2$	$\hat{-}$
	$b_{3-}\|3/2,-1/2\rangle + b_{3+}\|1/2,1/2\rangle$	$\|b_{3-}\|^2$	$\hat{-}$
$a_{2-}\|3/2,-1/2\rangle + a_{2+}\|1/2,1/2\rangle$	$\|3/2,1/2\rangle$	$\|a_{2-}\|^2$	$\hat{+}$
	$b_{4-}\|1/2,-1/2\rangle + b_{4+}\|-1/2,1/2\rangle$	$\|a_{2+}\|^2\|b_{4-}\|^2$	$\hat{-}$
	$b_{5-}\|1/2,-1/2\rangle + b_{5+}\|-1/2,1/2\rangle$	$\|a_{2+}\|^2\|b_{5-}\|^2$	$\hat{-}$
$a_{3-}\|3/2,-1/2\rangle + a_{3+}\|1/2,1/2\rangle$	$\|3/2,1/2\rangle$	$\|a_{3-}\|^2$	$\hat{+}$
	$b_{4-}\|1/2,-1/2\rangle + b_{4+}\|-1/2,1/2\rangle$	$\|a_{3+}\|^2\|b_{4-}\|^2$	$\hat{-}$
	$b_{5-}\|1/2,-1/2\rangle + b_{5+}\|-1/2,1/2\rangle$	$\|a_{3+}\|^2\|b_{5-}\|^2$	$\hat{-}$
$a_{4-}\|1/2,-1/2\rangle + a_{4+}\|-1/2,1/2\rangle$	$b_{2-}\|3/2,-1/2\rangle + b_{2+}\|1/2,1/2\rangle$	$\|a_{4-}\|^2\|b_{2+}\|^2$	$\hat{+}$
	$b_{3-}\|3/2,-1/2\rangle + b_{3+}\|1/2,1/2\rangle$	$\|a_{4-}\|^2\|b_{3+}\|^2$	$\hat{+}$
	$b_{6-}\|-1/2,-1/2\rangle + b_{6+}\|-3/2,1/2\rangle$	$\|a_{4+}\|^2\|b_{6-}\|^2$	$\hat{-}$
	$b_{7-}\|-1/2,-1/2\rangle + b_{7+}\|-3/2,1/2\rangle$	$\|a_{4+}\|^2\|b_{7-}\|^2$	$\hat{-}$
$a_{5-}\|1/2,-1/2\rangle + a_{5+}\|-1/2,1/2\rangle$	$b_{2-}\|3/2,-1/2\rangle + b_{2+}\|1/2,1/2\rangle$	$\|a_{5-}\|^2\|b_{2+}\|^2$	$\hat{+}$
	$b_{3-}\|3/2,-1/2\rangle + b_{3+}\|1/2,1/2\rangle$	$\|a_{5-}\|^2\|b_{3+}\|^2$	$\hat{+}$
	$b_{6-}\|-1/2,-1/2\rangle + b_{6+}\|-3/2,1/2\rangle$	$\|a_{5+}\|^2\|b_{6-}\|^2$	$\hat{-}$
	$b_{7-}\|-1/2,-1/2\rangle + b_{7+}\|-3/2,1/2\rangle$	$\|a_{5+}\|^2\|b_{7-}\|^2$	$\hat{-}$
$a_{6-}\|-1/2,-1/2\rangle + a_{6+}\|-3/2,1/2\rangle$	$b_{4-}\|1/2,-1/2\rangle + b_{4+}\|-1/2,1/2\rangle$	$\|a_{6-}\|^2\|b_{4+}\|^2$	$\hat{+}$
	$b_{5-}\|1/2,-1/2\rangle + b_{5+}\|-1/2,1/2\rangle$	$\|a_{6-}\|^2\|b_{5+}\|^2$	$\hat{+}$
	$\|-3/2,-1/2\rangle$	$\|a_{6+}\|^2$	$\hat{-}$
$a_{7-}\|-1/2,-1/2\rangle + a_{7+}\|-3/2,1/2\rangle$	$b_{4-}\|1/2,-1/2\rangle + b_{4+}\|-1/2,1/2\rangle$	$\|a_{7-}\|^2\|b_{4+}\|^2$	$\hat{+}$
	$b_{5-}\|1/2,-1/2\rangle + b_{5+}\|-1/2,1/2\rangle$	$\|a_{7-}\|^2\|b_{5+}\|^2$	$\hat{+}$
	$\|-3/2,-1/2\rangle$	$\|a_{7+}\|^2$	$\hat{-}$
$\|-3/2,-1/2\rangle$	$b_{6-}\|-1/2,-1/2\rangle + b_{6+}\|-3/2,1/2\rangle$	$\|b_{6+}\|^2$	$\hat{+}$
	$b_{7-}\|-1/2,-1/2\rangle + b_{7+}\|-3/2,1/2\rangle$	$\|b_{7+}\|^2$	$\hat{+}$

Table 5. D_2 Allowed Transitions F_1 and F_2 Values and Polarization

$^2S_{1/2}$	$^2P_{3/2}$	F_1F_2	Pol.
$\|3/2,1/2\rangle$	$\|3/2,3/2\rangle$	1/4	$\hat{+}$
	$b_{4,-0.5}\|3/2,-1/2\rangle+b_{4,0.5}\|1/2,1/2\rangle+b_{4,1.5}\|-1/2,3/2\rangle$	$\|b_{4,-0.5}\|^2/12$	$\hat{-}$
	$b_{5,-0.5}\|3/2,-1/2\rangle+b_{5,0.5}\|1/2,1/2\rangle+b_{5,1.5}\|-1/2,3/2\rangle$	$\|b_{5,-0.5}\|^2/12$	$\hat{-}$
	$b_{6,-0.5}\|3/2,-1/2\rangle+b_{6,0.5}\|1/2,1/2\rangle+b_{6,1.5}\|-1/2,3/2\rangle$	$\|b_{6,-0.5}\|^2/12$	$\hat{-}$
$a_{2-}\|3/2,-1/2\rangle+a_{2+}\|1/2,1/2\rangle$	$b_{2,0.5}\|3/2,1/2\rangle+b_{2,1.5}\|1/2,3/2\rangle$	$\|a_{2-}\|^2\|b_{2,0.5}\|^2/12+\|a_{2+}\|^2\|b_{2,1.5}\|^2/4$	$\hat{+}$
	$b_{3,0.5}\|3/2,1/2\rangle+b_{3,1.5}\|1/2,3/2\rangle$	$\|a_{2-}\|^2\|b_{3,0.5}\|^2/12+\|a_{2+}\|^2\|b_{3,1.5}\|^2/4$	$\hat{+}$
	$b_{7,-1.5}\|3/2,-3/2\rangle+b_{7,-0.5}\|1/2,-1/2\rangle$ $+b_{7,0.5}\|-1/2,1/2\rangle+b_{7,1.5}\|-3/2,3/2\rangle$	$\|a_{2-}\|^2\|b_{7,-1.5}\|^2/4+\|a_{2+}\|^2\|b_{7,-0.5}\|^2/12$	$\hat{-}$
	$b_{8,-1.5}\|3/2,-3/2\rangle+b_{8,-0.5}\|1/2,-1/2\rangle$ $+b_{8,0.5}\|-1/2,1/2\rangle+b_{8,1.5}\|-3/2,3/2\rangle$	$\|a_{2-}\|^2\|b_{8,-1.5}\|^2/4+\|a_{2+}\|^2\|b_{8,-0.5}\|^2/12$	$\hat{-}$
	$b_{9,-1.5}\|3/2,-3/2\rangle+b_{9,-0.5}\|1/2,-1/2\rangle$ $+b_{9,0.5}\|-1/2,1/2\rangle+b_{9,1.5}\|-3/2,3/2\rangle$	$\|a_{2-}\|^2\|b_{9,-1.5}\|^2/4+\|a_{2+}\|^2\|b_{9,-0.5}\|^2/12$	$\hat{-}$
	$b_{10,-1.5}\|3/2,-3/2\rangle+b_{10,-0.5}\|1/2,-1/2\rangle+$ $b_{10,0.5}\|-1/2,1/2\rangle+b_{10,1.5}\|-3/2,3/2\rangle$	$\|a_{2-}\|^2\|b_{10,-1.5}\|^2/4+\|a_{2+}\|^2\|b_{10,-0.5}\|^2/12$	$\hat{-}$
$a_{3-}\|3/2,-1/2\rangle+a_{3+}\|1/2,1/2\rangle$	$b_{2,0.5}\|3/2,1/2\rangle+b_{2,1.5}\|1/2,3/2\rangle$	$\|a_{3-}\|^2\|b_{2,0.5}\|^2/12+\|a_{3+}\|^2\|b_{2,1.5}\|^2/4$	$\hat{+}$
	$b_{3,0.5}\|3/2,1/2\rangle+b_{3,1.5}\|1/2,3/2\rangle$	$\|a_{3-}\|^2\|b_{3,0.5}\|^2/12+\|a_{3+}\|^2\|b_{3,1.5}\|^2/4$	$\hat{+}$
	$b_{7,-1.5}\|3/2,-3/2\rangle+b_{7,-0.5}\|1/2,-1/2\rangle+$ $b_{7,0.5}\|-1/2,1/2\rangle+b_{7,1.5}\|-3/2,3/2\rangle$	$\|a_{3-}\|^2\|b_{7,-1.5}\|^2/4+\|a_{3+}\|^2\|b_{7,-0.5}\|^2/12$	$\hat{-}$
	$b_{8,-1.5}\|3/2,-3/2\rangle+b_{8,-0.5}\|1/2,-1/2\rangle+$ $b_{8,0.5}\|-1/2,1/2\rangle+b_{8,-1.5}\|-3/2,3/2\rangle$	$\|a_{3-}\|^2\|b_{8,-1.5}\|^2/4+\|a_{3+}\|^2\|b_{8,-0.5}\|^2/12$	$\hat{-}$
	$b_{9,-1.5}\|3/2,-3/2\rangle+b_{9,-0.5}\|1/2,-1/2\rangle+$ $b_{9,0.5}\|-1/2,1/2\rangle+b_{9,1.5}\|-3/2,3/2\rangle$	$\|a_{3-}\|^2\|b_{10,-1.5}\|^2/4+\|a_{3+}\|^2\|b_{10,-0.5}\|^2/12$	$\hat{-}$
	$b_{10,-1.5}\|3/2,-3/2\rangle+b_{10,-0.5}\|1/2,-1/2\rangle+$ $b_{10,0.5}\|-1/2,1/2\rangle+b_{10,1.5}\|-3/2,3/2\rangle$	$\|a_{3-}\|^2\|b_{10,-1.5}\|^2/4+\|a_{3+}\|^2\|b_{10,-0.5}\|^2/12$	$\hat{-}$
$a_{4-}\|1/2,-1/2\rangle+a_{4+}\|-1/2,1/2\rangle$	$b_{4,-0.5}\|3/2,-1/2\rangle+b_{4,0.5}\|1/2,1/2\rangle+b_{4,1.5}\|-1/2,3/2\rangle$	$\|a_{4-}\|^2\|b_{4,0.5}\|^2/12+\|a_{4+}\|^2\|b_{4,1.5}\|^2/4$	$\hat{+}$
	$b_{5,-0.5}\|3/2,-1/2\rangle+b_{5,0.5}\|1/2,1/2\rangle+b_{5,1.5}\|-1/2,3/2\rangle$	$\|a_{4-}\|^2\|b_{5,0.5}\|^2/12+\|a_{4+}\|^2\|b_{5,1.5}\|^2/4$	$\hat{+}$
	$b_{6,-0.5}\|3/2,-1/2\rangle+b_{6,0.5}\|1/2,1/2\rangle+b_{6,1.5}\|-1/2,3/2\rangle$	$\|a_{4-}\|^2\|b_{6,0.5}\|^2/12+\|a_{4+}\|^2\|b_{6,1.5}\|^2/4$	$\hat{+}$
	$b_{11,-1.5}\|1/2,-3/2\rangle+b_{11,-0.5}\|-1/2,-1/2\rangle+$ $b_{11,0.5}\|-3/2,1/2\rangle$	$\|a_{4-}\|^2\|b_{11,-1.5}\|^2/4+\|a_{4+}\|^2\|b_{11,-0.5}\|^2/12$	$\hat{-}$
	$b_{12,-1.5}\|1/2,-3/2\rangle+b_{12,-0.5}\|-1/2,-1/2\rangle+$ $b_{12,0.5}\|-3/2,1/2\rangle$	$\|a_{4-}\|^2\|b_{12,-1.5}\|^2/4+\|a_{4+}\|^2\|b_{12,-0.5}\|^2/12$	$\hat{-}$
	$b_{13,-1.5}\|1/2,-3/2\rangle+b_{13,-0.5}\|-1/2,-1/2\rangle+$ $b_{13,0.5}\|-3/2,1/2\rangle$	$\|a_{4-}\|^2\|b_{13,-1.5}\|^2/4+\|a_{4+}\|^2\|b_{13,-0.5}\|^2/12$	$\hat{-}$
$a_{5-}\|1/2,-1/2\rangle+a_{5+}\|-1/2,1/2\rangle$	$b_{4,-0.5}\|3/2,-1/2\rangle+b_{4,0.5}\|1/2,1/2\rangle+b_{4,1.5}\|-1/2,3/2\rangle$	$\|a_{5-}\|^2\|b_{4,0.5}\|^2/12+\|a_{5+}\|^2\|b_{4,1.5}\|^2/4$	$\hat{+}$
	$b_{5,-0.5}\|3/2,-1/2\rangle+b_{5,0.5}\|1/2,1/2\rangle+b_{5,1.5}\|-1/2,3/2\rangle$	$\|a_{5-}\|^2\|b_{5,0.5}\|^2/12+\|a_{5+}\|^2\|b_{5,1.5}\|^2/4$	$\hat{+}$
	$b_{6,-0.5}\|3/2,-1/2\rangle+b_{6,0.5}\|1/2,1/2\rangle+b_{6,1.5}\|-1/2,3/2\rangle$	$\|a_{5-}\|^2\|b_{6,0.5}\|^2/12+\|a_{5+}\|^2\|b_{6,1.5}\|^2/4$	$\hat{+}$
	$b_{11,-1.5}\|1/2,-3/2\rangle+b_{11,-0.5}\|-1/2,-1/2\rangle+$ $b_{11,0.5}\|-3/2,1/2\rangle$	$\|a_{5-}\|^2\|b_{11,-1.5}\|^2/4+\|a_{5+}\|^2\|b_{11,-0.5}\|^2/12$	$\hat{-}$
	$b_{12,-1.5}\|1/2,-3/2\rangle+b_{12,-0.5}\|-1/2,-1/2\rangle+$ $b_{12,0.5}\|-3/2,1/2\rangle$	$\|a_{5-}\|^2\|b_{12,-1.5}\|^2/4+\|a_{5+}\|^2\|b_{12,-0.5}\|^2/12$	$\hat{-}$
	$b_{13,-1.5}\|1/2,-3/2\rangle+b_{13,-0.5}\|-1/2,-1/2\rangle+$ $b_{13,0.5}\|-3/2,1/2\rangle$	$\|a_{5-}\|^2\|b_{13,-1.5}\|^2/4+\|a_{5+}\|^2\|b_{13,-0.5}\|^2/12$	$\hat{-}$
$a_{6-}\|-1/2,-1/2\rangle+a_{6+}\|-3/2,1/2\rangle$	$b_{7,-1.5}\|3/2,-3/2\rangle+b_{7,-0.5}\|1/2,-1/2\rangle+$ $b_{7,0.5}\|-1/2,1/2\rangle+b_{7,1.5}\|-3/2,3/2\rangle$	$\|a_{6-}\|^2\|b_{7,0.5}\|^2/12+\|a_{6+}\|^2\|b_{7,1.5}\|^2/4$	$\hat{+}$
	$b_{8,-1.5}\|3/2,-3/2\rangle+b_{8,-0.5}\|1/2,-1/2\rangle+$ $b_{8,0.5}\|-1/2,1/2\rangle+b_{8,1.5}\|-3/2,3/2\rangle$	$\|a_{6-}\|^2\|b_{8,0.5}\|^2/12+\|a_{6+}\|^2\|b_{8,1.5}\|^2/4$	$\hat{+}$
	$b_{9,-1.5}\|3/2,-3/2\rangle+b_{9,-0.5}\|1/2,-1/2\rangle+$ $b_{9,0.5}\|-1/2,1/2\rangle+b_{9,1.5}\|-3/2,3/2\rangle$	$\|a_{6-}\|^2\|b_{9,0.5}\|^2/12+\|a_{6+}\|^2\|b_{9,1.5}\|^2/4$	$\hat{+}$
	$b_{10,-1.5}\|3/2,-3/2\rangle+b_{10,-0.5}\|1/2,-1/2\rangle+$ $b_{10,0.5}\|-1/2,1/2\rangle+b_{10,1.5}\|-3/2,3/2\rangle$	$\|a_{6-}\|^2\|b_{10,0.5}\|^2/12+\|a_{6+}\|^2\|b_{10,1.5}\|^2/4$	$\hat{+}$
	$b_{14,-1.5}\|-1/2,-3/2\rangle+b_{14,-0.5}\|-3/2,-1/2\rangle$	$\|a_{6-}\|^2\|b_{14,-1.5}\|^2/4+\|a_{6+}\|2\|b_{14,-0.5}\|^2/12$	$\hat{-}$
	$b_{15,-1.5}\|-1/2,-3/2\rangle+b_{15,-0.5}\|-3/2,-1/2\rangle$	$\|a_{6-}\|^2\|b_{15,-1.5}\|^2/4+\|a_{6+}\|^2\|b_{15,-0.5}\|^2/12$	$\hat{-}$
$a_{7-}\|-1/2,-1/2\rangle+a_{7+}\|-3/2,1/2\rangle$	$b_{7,-1.5}\|3/2,-3/2\rangle+b_{7,-0.5}\|1/2,-1/2\rangle+$ $b_{7,0.5}\|-1/2,1/2\rangle+b_{7,1.5}\|-3/2,3/2\rangle$	$\|a_{7-}\|^2\|b_{7,0.5}\|^2/12+\|a_{7+}\|^2\|b_{7,1.5}\|^2/4$	$\hat{+}$

Table 5. (*Continued*)

$^2S_{1/2}$	$^2P_{3/2}$	F_1F_2	Pol.
	$b_{8,-1.5}\|3/2,-3/2\rangle+b_{8,-0.5}\|1/2,-1/2\rangle+b_{8,0.5}\|-1/2,1/2\rangle+b_{8,1.5}\|-3/2,3/2\rangle$	$\|a_{7-}\|^2\|b_{8,0.5}\|^2/12+\|a_{7+}\|^2\|b_{8,1.5}\|^2/4$	$\hat{+}$
	$b_{9,-1.5}\|3/2,-3/2\rangle+b_{9,-0.5}\|1/2,-1/2\rangle+b_{9,0.5}\|-1/2,1/2\rangle+b_{9,1.5}\|-3/2,3/2\rangle$	$\|a_{7-}\|^2\|b_{9,0.5}\|^2/12+\|a_{7+}\|^2\|b_{9,1.5}\|^2/4$	$\hat{+}$
	$b_{10,-1.5}\|3/2,-3/2\rangle+b_{10,-0.5}\|1/2,-1/2\rangle+b_{10,0.5}\|-1/2,1/2\rangle+b_{10,1.5}\|-3/2,3/2\rangle$	$\|a_{7-}\|^2\|b_{10,0.5}\|^2/12+\|a_{7+}\|^2\|b_{10,1.5}\|^2/4$	$\hat{+}$
	$b_{14,-1.5}\|-1/2,-3/2\rangle+b_{14,-0.5}\|-3/2,-1/2\rangle$	$\|a_{7-}\|^2\|b_{14,-1.5}\|^2/4+\|a_{7+}\|^2\|b_{14,-0.5}\|^2/12$	$\hat{-}$
	$b_{15,-1.5}\|-1/2,-3/2\rangle+b_{15,-0.5}\|-3/2,-1/2\rangle$	$\|a_{7-}\|^2\|b_{15,-1.5}\|^2/4+\|a_{7+}\|^2\|b_{15,-0.5}\|^2/12$	$\hat{-}$
$\|-3/2,-1/2\rangle$	$b_{11,-1.5}\|1/2,-3/2\rangle+b_{11,-0.5}\|-1/2,-1/2\rangle+b_{11,0.5}\|-3/2,1/2\rangle$	$\|b_{11,0.5}\|^2/12$	$\hat{+}$
	$b_{12,-1.5}\|1/2,-3/2\rangle+b_{12,-0.5}\|-1/2,-1/2\rangle+b_{12,0.5}\|-3/2,1/2\rangle$	$\|b_{12,0.5}\|^2/12$	$\hat{+}$
	$b_{13,-1.5}\|1/2,-3/2\rangle+b_{13,-0.5}\|-1/2,-1/2\rangle+b_{13,0.5}\|-3/2,1/2\rangle$	$\|b_{13,0.5}\|^2/12$	$\hat{+}$
	$\|-3/2,-3/2\rangle$	1/4	$\hat{+}$

$$\begin{bmatrix} l' & J' & S \\ J & l & 1 \end{bmatrix}$$

is the 6-j symbol; their values are from Tables 5 and 6 in Edmonds [34]. F_1 and F_2 are defined as

$$F_1 = |a|^2|b|^2,$$

$$F_2 = \begin{pmatrix} J' & 1 & J \\ -m_J' & \pm 1 & m_J \end{pmatrix}^2. \tag{A6}$$

These probabilities are tabulated for the Na and K Zeeman-split hyperfine transitions for each circular polarization component of the $^2P_{1/2} \rightarrow {}^2S_{1/2}$ (D_1) and $^2P_{3/2} \rightarrow {}^2S_{1/2}$ (D_2) transitions, as discussed below. Note that with the choice of the $|I,J,m_I,m_J\rangle$ base states, the electronic dipole moments of the transitions are independent from the nuclear spin of the system.

2. D_1 Transition Probabilities of Allowed Transitions

For this transition $J'=1/2$, $J=1/2$, $l'=1$ (P-state), $l=0$ (S-state), and $S=1/2$. By inserting these values into Eq. (A5), the transition probability is found to be

$$|\langle m_I' m_J' | p_\pm | m_I m_J \rangle|^2 = F_1 F_2 \frac{2}{3} S_0, \tag{A7}$$

with $F_2=1/3$ from Eq. (A6). Table 4 shows the values of F_1 of the allowed transitions, as well as for which $\sigma_\pm$ circular polarization. The subscripts on the a and b coefficients represent which state and m_J value they correspond to.

3. D_2 Transition Probabilities of Allowed Transitions

For this transition $J'=3/2$, $J=1/2$, $l'=1$ (P-state), $l=0$ (S-state), and $S=1/2$. By inserting these values into Eq. (A5), the transition probability is found to be

$$|\langle m_I' m_J' | p_\pm | m_I m_J \rangle|^2 = F_1 F_2 \frac{4}{3} S_0, \tag{A8}$$

where $F_2=1/12$ or $1/4$, depending on whether $|m_J'|=1/2$, or $3/2$, respectively, as indicated in Table 5. Table 5 shows the values of F_1F_2 of the allowed transitions, as well as the $\sigma_\pm$ circular polarization. The subscripts on the a and b coefficients represent which state and m_J value they correspond to.

ACKNOWLEDGMENTS

The work at Colorado State University was partially supported by a National Science Foundation (NSF) grant ATM-0804295.

REFERENCES

1. D. J. Dick and T. M. Shay, "Ultrahigh-noise rejection optical filter," Opt. Lett. **16**, 867–869 (1991).
2. Y. Ohman, "On some new auxiliary instruments in astrophysical research VI. A tentative monochromator for solar work based on the principle of selective magnetic rotation," Stockholms Obs. Ann. **19**(4), 9–11 (1956).
3. J. Menders, K. Benson, S. H. Bloom, C. S. Liu, and E. Korevaar, "Ultranarrow line filtering using a Cs Faraday filter at 852 nm," Opt. Lett. **16**, 846–848 (1991).
4. Y. C. Chan and J. A. Gelbwachs, "A Fraunhofer-wavelength magnetooptic atomic filter at 422.7 nm," IEEE J. Quantum Electron. **29**, 2379–2384 (1993).
5. G. Agnelli, A. Cacciani, and M. Fofi, "The magneto-optical filter I," Sol. Phys. **44**, 509–518 (1975).
6. H. Chen, C. Y. She, P. Searcy, and E. Korevaar, "Sodium-vapor dispersive Faraday filter," Opt. Lett. **18**, 1019–1021 (1993).
7. Z. Hu, X. Sun, Y. Liu, L. Fu, and X. Zeng, "Temperature properties of Na dispersive Faraday optical filter at D_1 and D_2 line," Opt. Commun. **156**, 289–293 (1998).
8. Y. Zhang, X. Jia, Z. Ma, and Q. Wang, "Optical filtering characteristics of potassium Faraday optical filter," IEEE J. Quantum Electron. **37**, 372–375 (2001).
9. H. Chen, M. A. White, D. A. Krueger, and C. Y. She, "Daytime mesopause temperature measurements with a sodium-vapor dispersive Faraday filter in a lidar receiver," Opt. Lett. **21**, 1093–1095 (1996).

10. C. Y. She, T. Li, R. L. Collins, T. Yuan, B. P. Williams, T. D. Kawahara, J. D. Vance, P. Acott, D. A. Krueger, H.-L. Liu, and M. E. Hagan, "Tidal perturbations and variability in the mesopause region over Fort Collins, CO (41 N, 105 W): Continuous multi-day temperature and wind lidar observations," Geophys. Res. Lett. **31**, L24111 (2004).
11. T. G. Slanger, P. C. Cosby, D. L. Huestis, A. Saiz-Lopez, B. J. Murray, D. A. O'Sullivan, J. M. C. Plane, C. Allende Prieto, F. J. Martin-Torres, and P. Jenniskens, "Variability of the mesospheric nightglow sodium D_2/D_1 ratio," J. Geophys. Res. **110**, D23302 (2005).
12. P. Yeh, "Dispersive magnetooptic filters," Appl. Opt. **21**, 2069–2075 (1982).
13. D. A. Van Baak, "Resonant Faraday rotation as a probe of atomic dispersion," Am. J. Phys. **64**, 724–735 (1996).
14. E. T. Dressler, A. E. Laux, and R. I. Billmers, "Theory and experiment for the anomalous Faraday effect in potassium," J. Opt. Soc. Am. B **13**, 1849–1857 (1996).
15. B. Yin and T. M. Shay, "Theoretical model for a Faraday anomalous dispersion optical filter," Opt. Lett. **16**, 1617–1619 (1991).
16. J. J. Sakurai, *Modern Quantum Mechanics* (Addison-Wesley, 1994), Revised Ed., pp. 176–181.
17. F. Schreier, "The Voigt and complex error function: A comparison of computational methods," J. Quant. Spectrosc. Radiat. Transf. **48**, 743–762 (1992).
18. A. Corney, *Atomic and Laser Spectroscopy* (Clarendon Press, 1977), pp. 667–674.
19. Ref. [18] p. 87.
20. Interactive Data Language (ITT Corporation, Boulder, Colorado).
21. K. S. Krane, *Introductory Nuclear Physics* (Wiley, 1988), pp. 602–651.
22. Ref. [21] pp. 822–833.
23. N. J. Stone, "Table of nuclear magnetic dipole and electric quadrupole moments," At. Data Nucl. Data Tables **90**, 75–176 (2005).
24. E. Arimondo, M. Inguscio, and P. Violino, "Experimental determinations of the hyperfine structure in the alkali atoms," Rev. Mod. Phys. **49**, 31–75 (1977).
25. S. Falke, E. Tiemann, and C. Lisdat, "Transition frequencies of the *D* lines of ^{39}K, ^{40}K, and ^{41}K measured with a femtosecond laser frequency comb," Phys. Rev. A **74**, 032503 (2006).
26. W. A. Van Wijngaarden and J. Li, "Measurement of hyperfine structure of sodium $3P_{1/2,3/2}$ states using optical spectroscopy," Z. Phys. D: At., Mol. Clusters **32**, 67–71 (1994).
27. Y. P. Gangrsky, D. V. Karaivanov, K. P. Marinova, B. N. Markov, L. M. Melnikova, G. V. Mishinsky, S. G. Zemlyanoi, and V. I. Zhemenik, "Hyperfine splitting and isotope shift in the atomic D_2 line of ^{22,23}Na and the quadrupole moment of ^{22}Na," Eur. Phys. J. A **3**, 313–318 (1998).
28. Yu. Ralchenko, A. E. Kramida, J. Reader, and NIST ASD Team, "NIST Atomic Spectra Database" (National Institute of Standards and Technology, Gaithersburg, MD, 2008), version 3.1.4, ⟨http://physics.nist.gov/asd3⟩.
29. W. L. Wiese, M. W. Smith, and B. M. Miles, "Atomic Transition Probabilities: Volume II, Sodium Through Calcium," Nat. Stand. Ref. Data Ser., Nat. Bur. Stand. (U. S.), 22.
30. R. E. Honig and D. A. Kramer, "Vapor pressure data for the solid and liquid elements," RCA Rev. **30**, 285–305 (1969).
31. W. Huang, X. Chu, B. P. Williams, S. D. Harrell, and J. Wiig, "Na double-edge magneto-optic filter for Na lidar profiling of wind and temperature in the lower atmosphere," Opt. Lett. **34**, 199–201 (2009).
32. A. R. Edmonds, *Angular Momentum in Quantum Mechanics* (Princeton U. Press, 1957), pp. 75–76.
33. Ref. [32] p. 111.
34. Ref. [32] pp. 125–127, 130–132.